Oxidation of α-methylphenylglycine under Fenton and electro-Fenton conditions in the dark and in the presence of solar light

Anna Serra [a], Xavier Domènech [a], Conchita Arias [b], Enric Brillas [b,*], José Peral [a,**]

[a] Departament de Química, Edifici Cn, Universitat Autònoma de Barcelona, E-08193 Bellaterra, Barcelona, Spain
[b] Laboratori d'Electroquímica dels Materials i del Medi Ambient, Departament de Química Física, Facultat de Química, Universitat de Barcelona, Martí i Franquès 1-11, 08028 Barcelona, Spain

ARTICLE INFO

ABSTRACT

The oxidation of α-methylphenylglycine (α-MPG, S-2-amino-2-phenylpropionic acid) amino acid in aqueous solution by means of Fenton, solar photo-Fenton (SPF), electro-Fenton (EF), and solar photoelectro-Fenton (SPEF) reactions is studied. Several H_2O_2 initial concentrations were used in the chemical systems, while different currents were tested in the electrochemical ones where H_2O_2 was electrogenerated from O_2 reduction at a gas diffusion cathode. α-MPG concentration and total organic carbon (TOC) removals along time were ascertained, and the electrochemical reactions turned out to be faster than the chemical ones. The presence of light was beneficial for both configurations. Reaction intermediates were detected using high-performance liquid chromatography, gas chromatography–mass spectrometry, and liquid chromatography–mass spectrometry analysis. A special attention was paid to the nature and time course of the carboxylic acids generated, being oxalic and oxamic acids those detected at higher concentrations. Apart from oxamic acid, NH_4^+ and NO_3^- ions were the nitrogen containing species detected and the nitrogen mass balance was not closed, probably due to the generation of NO_x or other volatile nitrogen species. Taking into account all the collected information about the reaction intermediates, a comprehensive reaction mechanism for α-MPG oxidation to aromatic intermediates is proposed.
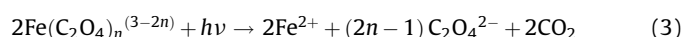
1. Introduction

Many aqueous pollutants are of organic nature and they can be potentially degraded through the use of powerful oxidants. Indeed, in the last years, several oxidation reactions grouped under the name of Advanced Oxidation Processes (AOPs) have been studied for the removal of toxic and/or non-biodegradable organics in wastewaters [1–3]. They all have in common the generation of highly reactive radical species related to the hydroxyl radical (HO•), a powerful oxidant with a high standard redox potential ($E°(•OH/H_2O) = 2.80$ V vs. NHE) that non-selectively react with most organics taking them to total mineralization, i.e., total conversion into CO_2, water and inorganic ions. The AOPs are environment friendly chemical, photochemical, photocatalytic and electrochemical procedures. Many of those reactions are clearly improved by the use of light, and many research efforts are underway to develop solar light driven techniques that allow the use of cheap solar photons of wavelengths longer than 300 nm.

One of the most studied AOPs is the classical Fenton reaction:

$$Fe^{2+} + H_2O_2 \rightarrow Fe^{3+} + HO^• + OH^- \tag{1}$$
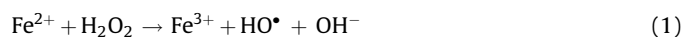
where HO• is generated from the reaction between an Fe^{2+} salt and H_2O_2 [4–6]. This is a rather inexpensive and easy to handle procedure that can be used to efficiently oxidize a wide variety of organics. The chemical attack is normally accelerated in the presence of UVA light, and two reasons seem to account for such a behaviour: (i) the photolysis of the $Fe(OH)^{2+}$ complex (the predominant species of Fe(III) in aqueous solution at pH 3), named photo-Fenton (PF) reaction (see Eq. (2) [7–9]), which regenerates the Fe^{2+} catalyst and generates more HO•; and (ii) the photolysis of complexes formed between Fe(III) and oxidation by-products such as oxalic (see Eq. (3) [10]) and other carboxylic acids:

$$Fe(OH)^{2+} + h\nu \rightarrow Fe^{2+} + HO^• \tag{2}$$

$$2Fe(C_2O_4)_n^{(3-2n)} + h\nu \rightarrow 2Fe^{2+} + (2n-1)\,C_2O_4^{2-} + 2CO_2 \tag{3}$$

Over the last decade, AOPs based on the use of electrochemical reactions have also been developed [11–24], specially the electro-Fenton (EF) process that involves the H_2O_2 electrogeneration through the two-electron reduction of O_2 at carbon-felt or a

* Corresponding author.
** Corresponding author. Tel.: +34 935 81 27 72; fax: +34 935 81 29 20.
   E-mail addresses: brillas@ub.edu (E. Brillas), jose.peral@uab.cat (J. Peral).

carbon-polytetrafluoroethylene (PTFE) O_2-diffusion cathode:

$$O_{2(g)} + 2H^+ + 2e^- \rightarrow H_2O_2 \tag{4}$$

and the addition of small amounts of Fe^{2+} to the solution to provide Fenton conditions (Eq. (1)). Since Fe^{3+} can be reduced to Fe^{2+} at the cathode [12], the Fenton reaction can be catalytically sustained through a fast conversion between Fe(II) and Fe(III). The most frequently used anodes in the indirect electro-oxidation EF systems are Pt and boron-doped diamond (BDD) [13,14,18,20–22], being the latter preferable by its higher oxidation power on organic pollutants. If the electrochemical process is carried out in an undivided cell, apart from the electro-Fenton mechanism, organics can also be destroyed by $HO^\bullet$ produced at the anode surface from water oxidation (reaction (5) in the case of a BDD anode [23]), or in much smaller extent with the weaker oxidant hydroperoxyl radical ($HO_2^\bullet$) electrogenerated from H_2O_2 oxidation on the anode (reaction (6) [24]):

$$BDD + H_2O \rightarrow BDD(HO^\bullet) + H^+ + e^- \tag{5}$$

$$BDD + H_2O_2 \rightarrow BDD(HO_2^\bullet) + H^+ + e^- \tag{6}$$
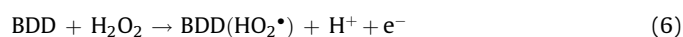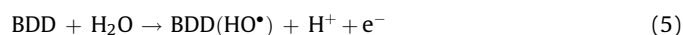
The electro-Fenton process can also be improved under light radiation of the contaminated solution. As mentioned above, light can additionally produce the photo-Fenton reaction and the photolysis of Fe(III)–organic complexes. Under those circumstances, the complex set of reactions that take place simultaneously is named photoelectro-Fenton (PEF) process [24,25].

Although based on the same fundamental reaction (Fenton reaction) and the use of the same oxidant ($HO^\bullet$), those photochemical and photoelectrochemical systems can be quite different in terms of kinetics, reaction efficiencies, and amounts of reagents and energy consumed. Thus, the decision about the best choice for a specific wastewater treatment always involves comparison between the different reactive configurations.

In this paper, the degradation of the α-methylphenylglycine (α-MPG, S-2-amino-2-phenylpropionic acid) amino acid in aqueous solution by Fenton, EF, solar driven photo-Fenton (SPF), and solar photoelectro-Fenton (SPEF) processes is studied. α-MPG is a common precursor of pharmaceuticals and was selected as an aromatic amino acid model molecule because of its high water solubility and its non-biodegradable character. The indirect electro-oxidation methods were conducted in a small undivided BDD/O_2 cell. All treatments were performed at pH 2.9 ± 0.1, close to the optimum pH of 2.8 for those AOPs [4,24,25], and in the presence of 10 mg L^{-1} of Fe^{2+} as catalyst (the maximum legal content of this species permitted by the Spanish legislation for wastewater disposal [26]). The effect of H_2O_2 initial concentration and applied current on the oxidation process, and the α-MPG and TOC removal kinetics for the four methods were explored. Although previous research concerning the degradation of α-MPG in homogeneous (photo-Fenton) and heterogeneous (TiO_2 photo-assisted) photocatalytic systems can be found [27–30] nothing has been said so far about the reaction mechanism in those conditions. In the present work a detailed study of the detected reaction intermediates, the evolution with time of carboxylic acids, and the mass balance of the N atom was carried out. From these results, a general α-MPG degradation pathway to aromatic intermediates, plausible for the four $HO^\bullet$-based techniques, is proposed.

2. Experimental

2.1. Chemicals

Pure α-MPG from DMS Deretil was used as received. Oxalic and oxamic acids were of analytical grade and purchased from Panreac

and Avocado, respectively. Reagent grade 33% (w/v) H_2O_2 was obtained from Panreac. Anhydrous sodium sulphate, employed as background electrolyte, and heptahydrated ferrous sulphate, used as catalyst, were of analytical grade and supplied by Fluka. Solutions were prepared with high-purity water from a Millipore Milli-Q system (resistivity > 18 MΩ cm at 25 °C) and the pH was hold to 2.9 ± 0.1 with analytical grade sulphuric acid from Merck. Organic solvents and other chemicals employed were either HPLC or analytical grade from Fluka, Panreac and Sigma–Aldrich.

2.2. Instruments and analytical procedures

Galvanostatic experiments were carried out with an Amel 2051 potentiostat–galvanostat, connected to a Kontron DMM655 multi-meter for the direct measurement of cell voltage. The solution pH was measured with a Crison 2000 pH-meter. Before analysis, all samples withdrawn from treated solutions were filtered with Whatman 0.45-μm PTFE filters.

The mineralization of α-MPG solutions was monitored by the removal of their TOC, determined on a Shimadzu VCSN TOC analyzer. Reproducible TOC values, with $\pm 1\%$ accuracy, were obtained by injecting 50 μL aliquots into the TOC analyzer. H_2O_2 concentration was determined from the light absorption of the titanic–hydrogen peroxide colored complex at $\lambda = 408$ nm [31], using a Unicam UV–vis UV4 spectrophotometer thermostated at 25 °C.

The amino acid decay was followed by reversed-phase HPLC chromatography with a Shimadzu 10Avp high-performance liquid chromatograph fitted with a Phenomenex Luna 5 μm C18 column (250 mm × 4.6 mm (i.d.)) at room temperature and coupled with a Shimadzu SPD-M10Avp diode array detector working at $\lambda = 220$ nm. This analysis was carried out by injecting 20 μL samples into the chromatograph using a 50-mM H_3PO_4 solution adjusted to pH 2.5 with NaOH at 0.7 mL min^{-1} as mobile phase. Under these conditions, the chromatogram displayed a well-defined absorption peak for α-MPG at a retention time (t_r) of 13.9 min. Generated carboxylic acids were followed by ion-exclusion HPLC chromatography using the above chromatograph fitted with a Bio-Rad Aminex HPX 87H column (300 mm × 7.8 mm (i.d.)) at 35 °C, along with the photodiode array detector at $\lambda = 210$ nm. In this technique, 20 μL samples were injected into the chromatograph and the mobile phase was 4 mM H_2SO_4 at 0.6 mL min^{-1}.

NH_4^+ and NO_3^- concentrations in treated solutions were determined by ion chromatography with the same HPLC chromatograph coupled with a Shimadzu CDD 10Avp conductivity detector. For NH_4^+ measurement, the chromatograph was fitted with a Shodex IC KY-421 cation column (125 mm × 4.6 mm (i.d.)) at 40 °C and the NH_4^+ peak appeared in the chromatogram at $t_r = 4.4$ min using a solution with 5 mM tartaric acid, 2 mM dipicolinic acid and 24.2 mM boric acid as mobile phase at 1.0 mL min^{-1}. For NO_3^- determination, a Shim-Pack IC-A1S anion column (100 mm × 4.6 mm (i.d.)) at 40 °C was utilized and the chromatogram displayed the corresponding peak at $t_r = 6.1$ min using an aqueous mobile phase with 1.0 mM p-hydroxybenzoic acid and 1.1 mM N,N-diethylethanolamine at 1.5 mL min^{-1}.

Aromatic intermediates produced between 10 and 60 min of several EF treatments at 300 mA were identified by GC–MS and LC–MS. The GC–MS technique was carried out with a Hewlett-Packard 5890 Series II gas chromatograph coupled to a Hewlett-Packard 5989. A mass spectrophotometer operating in electron impact (EI) mode at 70 eV. A NIFT05 data library was used to identify the mass spectra. The LC–MS technique was performed with an Agilent 1200 Series liquid chromatograph equipped with an Agilent 1200 Series UV detector at $\lambda = 220$ nm and coupled to an Applied Biosystems Q-STAR Elite mass spectrophotometer operating in ESI+. In all cases, a solid-phase extraction (SPE) was performed by consecutive

injection of 70 mL of the electrolyzed solution through an Oasis HLB or MCX cartridge and further, using 2 mL of an organic solvent as eluent. The following measurements were made: (a) a sample eluted with 2 mL of (1:1) methanol:dimethylether was directly analyzed by GC–MS using a polar column HP-Innowax 0.25 μm (30 m × 0.25 mm (i.d.)) with a temperature ramp of 50 °C for 3 min, 10 °C min^{-1} up to 300 °C and hold time 5 min, and a temperature for the injector and detector of 250 and 290 °C, respectively; (b) a sample eluted with 2 mL of methanol (or 2 mL of acetonitrile) was treated with 200 μL of N,O-bis-(trimethylsilyl)acetamide under stirring and heating at 60 °C for 20 min. The resulting methylsilylated derivatives were detected by GC–MS using a non-polar HP-5MS column with 5% phenyl methyl siloxane (30 m × 0.25 mm (i.d.)) under the same conditions stated above for the polar column; (c) a sample eluted with 2 mL of (1:1) methanol:dimethylether was rotavaporated to extract the organic solvents and the remaining products were dissolved in 1 mL of Milli-Q water to be further analyzed by LC–MS using the above Phenomenex Luna column circulating a 0.05% acetic acid solution at 0.4 mL min^{-1} at 40 °C as mobile phase.

Generated carboxylic acids formed after 40 min of EF treatment at 300 mA were also identified by GC–MS. 25 mL of the electrolyzed solution were lyophilized and the remaining solid was diluted with 2 mL of ethyl acetate and treated with 200 μL of the silylation agent as described above. The methylsilylated compounds thus obtained were detected and identified by GC–MS using the non-polar HP-5MS column with a temperature ramp of 80 °C for 1 min, 7 °C min^{-1} up to 150 °C, hold time 5 min, 7 °C min^{-1} up to 200 °C and hold time 5 min. The temperature of the injector and detector were 250 and 290 °C, respectively.

2.3. Reaction systems

All trials were carried out in open and cylindrical Pyrex glass reactors of 400 mL capacity. 250 mL solutions of pH 2.9 and containing 500 mg L^{-1} α-MPG and 10 mg L^{-1} Fe^{2+} were degraded in all cases. 0.05 M Na$_2$SO$_4$ as background electrolyte were always used in the electrochemical trials. During each run the solution was vigorously stirred with a magnetic bar to ensure its homogenization and suitable transport of reactants towards/from the electrodes. In all cases, the solution temperature was always maintained at 25 °C with a water circulation jacket connected to an external thermostat.

Electrochemical experiments were conducted with a 3-cm^2 BDD thin-film anode deposited on a conductive Si sheet from CSEM, and with a 3-cm^2 carbon-PTFE cathode from E-TEK, fed with pure O$_2$ at 10 L h^{-1}. The preparation of the O$_2$-diffusion cathode was described elsewhere [13]. The interelectrode gap was about 1 cm. The electrode surfaces were frequently cleaned from organic impurities and activated by electrolyzing a 0.05-M Na$_2$SO$_4$ solution of pH 3.0 at a current of 300 mA for 2 h.

The solar treatments were carried out under direct exposition of the cell to solar irradiation, with a mirror at its bottom to better concentrate the sun rays. Those trials were performed in sunny and clear days during the months of June–August of 2007 at the Barcelona laboratory (longitude: 41°21′ N, latitude: 2°10′ E), with a decay in solar irradiation intensity from about 1000 W m^{-2} at noon to 400 W m^{-2} at 17 h, yielding an average UV irradiation intensity close to 15 W m^{-2} (approximately 3.7 × 10^{19} photons m^{-2} s^{-1}) as measured by the university weather station.

3. Results and discussion

3.1. Comparative degradation

The oxidation of α-MPG has been carried out by using Fenton, SPF, EF, and SPEF techniques. As indicated in the previous section,

500 mg L^{-1} α-MPG solutions at pH 2.9 have been the target in all experiments. Preliminary runs were conducted in order to know the effect that different concentrations of Fe^{2+} had on the reaction efficiencies. In this sense, after 3 h of Fenton conditions using a initial H$_2$O$_2$ concentration of 145.0 mM, increasing quantities of 10, 20 and 30 mg L^{-1} of Fe^{2+} led to increasing TOC degradations of 23.1, 37.7, and 44.1%, respectively. The choice of the Fe^{2+} concentration used in the ensuing experiments involving Fenton reaction (1) was made taking into account two considerations: (a) a lower Fe^{2+} load is preferred in order to avoid high iron concentrations in the final treated effluent; and (b) the lower concentration used in this work (10 mg L^{-1}) gives a noticeable organic degradation in a reasonable time. Thus, 10 mg L^{-1} of Fe^{2+} appeared to be enough to efficiently catalyze the different Fenton derived processes and it was chosen for the rest of the experiments.

Fig. 1 compares the TOC removals obtained under Fenton and solar photo-Fenton conditions when using three different initial H$_2$O$_2$ concentrations that are equivalent to the stoichiometric (72.5 mM), twice the stoichiometric (145.0 mM), and half the stoichiometric (36.3 mM) amount of H$_2$O$_2$ needed for complete α-MPG mineralization, assuming overall release of initial nitrogen in the form of nitrate ion. Those H$_2$O$_2$ quantities were calculated by using Eq. (7):

$$C_9H_{11}NO_2 + 24H_2O_2 \rightarrow 9CO_2 + NO_3^- + H^+ + 29H_2O \qquad (7)$$

As can be seen in Fig. 1, TOC removals in Fenton experiments were clearly lower than in SPF experiments, and no important differences between Fenton experiments with the three different H$_2$O$_2$ concentrations were noticed. The H$_2$O$_2$ evolution along each experiment was also monitored (data not shown), and similar amounts of that chemical were consumed in Fenton experiments (around 26–28 mM). Thus, no clear benefit could be attributed to using larger quantities of this oxidant, being the Fenton process clearly controlled by the availability of Fe^{2+}. On the contrary, Fig. 1 shows an evident improvement on TOC removal in SPF trials when changing the H$_2$O$_2$ concentration from 36.3 to 72.5 mM. It is obvious that the faster recovery of the Fe^{2+} catalyst in the presence of sunlight (see Eq. (2)) involves a reaction rate controlled by the H$_2$O$_2$ concentration. Since a 36.3 mM concentration of such oxidant is not enough to mineralize the α-MPG, the reaction stops before complete TOC removal. However, no important differences exist between the 72.5 and 145.0 mM runs, indicating that, if the right H$_2$O$_2$ concentration is chosen, all the oxidant can

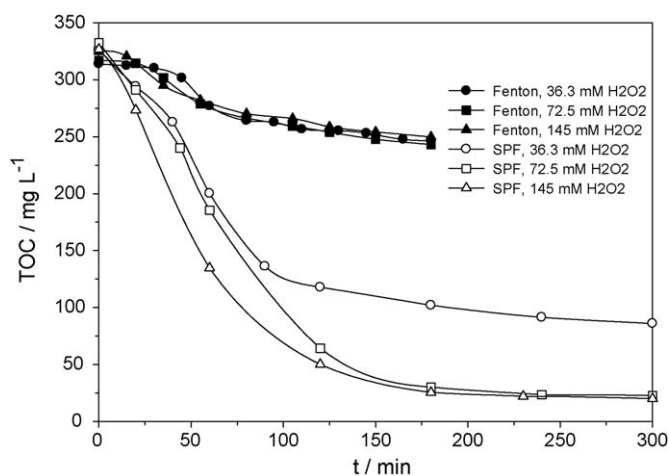**Fig. 1.** TOC decay during Fenton and solar photo-Fenton (SPF) experiments carried out with 500 mg L^{-1} α-MPG and 10 mg L^{-1} Fe^{2+} solutions at pH 2.9 and 25 °C. Initial H$_2$O$_2$ concentrations are indicated in the figure legend.

be efficiently consumed in the desired mineralization process. On the contrary, removal of all H_2O_2 was observed after 240 min of the three SPF experiments, pointing toward an unprofitable consumption of the H_2O_2 stoichiometric excess.

Another reason of the better performance of the solar photo-Fenton system is the existence of direct photolysis of the complexes formed between Fe^{3+} and some organic intermediates (especially those containing the carboxylic acid group) produced during the α-MPG degradation. The existence of such homogeneous photochemistry involving Fe(III)–carboxylic acid complexes has been previously described for other photo-Fenton systems [4,10]. As it will be reported later, oxalic acid is one of the main intermediates of the α-MPG degradation, and the photolysis of the iron–oxalate complex is a well-known process [32].

Fig. 2 compares the TOC removals obtained under EF and SPEF conditions. In those cases no H_2O_2 was initially added to the solution, being the oxidant electrochemically generated. Currents of 100, 300, and 450 mA were tested in order to generate different amounts of H_2O_2. As can be seen, the greater the current the larger TOC removal produced owing to the production of more heterogeneous $BDD(HO^\bullet)$ via reaction (5) and more homogeneous $HO^\bullet$ by the higher electrogeneration of H_2O_2, except in the cases of the SPEF experiments at 300 and 450 mA, with no noticeable differences existing. At 300 mA this system seems to arrive to saturation and further increase in current gives no TOC removal improvement. In any case it is obvious from Fig. 2 that the performance of the electrochemical system is improved by the presence of sunlight. After 8 h of EF process, 39.1, 22.9 and 14.9% of the initial TOC remain in solution for 100, 300 and 450 mA, respectively, while 6.8, 2.4 and 2.5% are the corresponding values after 5 h of SPEF treatment. Again, the faster recovery of Fe^{2+} through the PF reaction (2) and the existence of photolysis of the Fe(III)–carboxylic acid complexes can be used as a logical explanation of the beneficial role of sunlight.

A comparison between data of Figs. 1 and 2 seems to indicate that the electrochemical systems produce faster TOC removals than their chemical homologous. However, such a simple comparison cannot be carried out because differences exist between the H_2O_2 concentrations involved in chemical and electrochemical processes. To illustrate this point, quantification of the H_2O_2 concentrations present in solution along different electrochemical experiments at 300 mA were carried out (Fig. 3). Anodic oxidation of the background electrolyte in absence of α-MPG and Fe^{2+} salt in the BDD/O_2 cell gave an accumulation of H_2O_2 up to a steady value of 22 mM, indicating
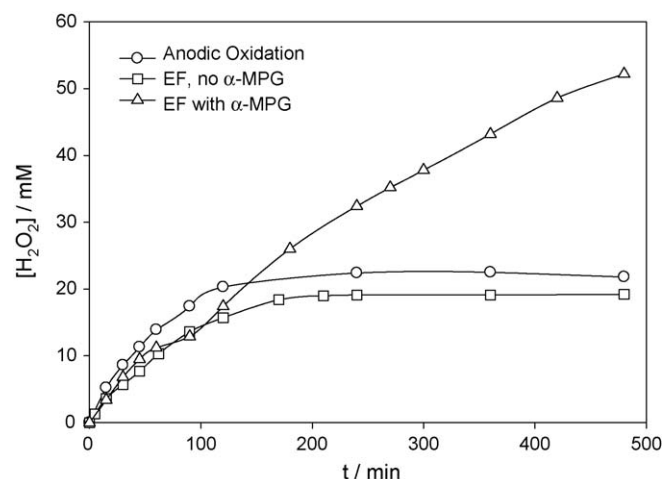
Fig. 3. H_2O_2 evolution in three different electrochemical experiments: ($\bigcirc$) anodic oxidation, ($\square$) EF with 10 mg L^{-1} Fe^{2+} and no α-MPG, and ($\triangle\Delta$) EF with 10 mg L^{-1} Fe^{2+} and 500 mg L^{-1} α-MPG. Other conditions: 300 mA, 0.05 M Na_2SO_4, pH 2.9 and 25 °C.

that the system was initially able to generate the oxidant, but that such generation was balanced with increasing rates of decomposition at the anode via reaction (6) for large enough H_2O_2 concentrations. The EF process with 10 mg L^{-1} Fe^{2+} in absence of α-MPG, also gave a steady H_2O_2 concentration of 19 mM, slightly lower because the presence of iron causes the existence of an additional H_2O_2 degradation pathway via Fenton reaction (1). However, EF and SPEF processes in the presence of α-MPG produced an always increasing H_2O_2 concentration in solution (no steady-state was attained), suggesting that, apart from consuming the oxidant, the α-MPG molecule also competes for some of the degradation routes slowing down the global H_2O_2 decomposition rate. Thus, while a fix concentration of H_2O_2 is initially added to the solution in Fenton-based experiments, this chemical is continuously generated and consumed in the EF based ones, being difficult to assess the total amount of H_2O_2 consumed along one electrochemical experiment. In other words, it makes no sense to compare quantities of H_2O_2 added in the pure chemical experiments with currents applied in the electrochemical ones and, thus, no clear conclusions about the efficiencies of both configurations in terms of H_2O_2 consumed per TOC removed can be adventured. An economical analysis of the expenses associated to H_2O_2 consumption in Fenton and SPF treatments, and the ones due to electrical consumption in EF and SPEF runs would be one possible way of efficiency comparison from a practical point of view. Also, due to the fact that H_2O_2 and electricity production are industrial activities that involve negative consequences to the environment, comparison of the chemical and the electrochemical processes could be performed in terms of environmental impacts of both processes. Further work based on the application of the Life Cycle Assessment tool [33] to the reactive systems described here would be the way to clarify this point.

In spite of the existing difficulties for a fair comparison of the chemical and the electrochemical systems, it seems reasonable to propose that alternative processes like the direct oxidation of α-MPG at the electrode can also explain the larger efficiencies of TOC removal observed for the electrochemical experiments.

The electrochemical reduction of Fe^{3+} and the fast recovery of Fe^{2+} had to be ruled out as an alternative potential explanation of the better electrochemical performance. Indeed, Fig. 4 shows the evolution of Fe (Fe^{2+} and Fe^{3+}) during a typical experiment within each technique. As can be seen, the general trend is that Fe^{2+} concentration rapidly decreases while the opposite occurs with Fe^{3+}, and fairly steady concentrations of both species are detected after approximately 30 min. However the final concentrations
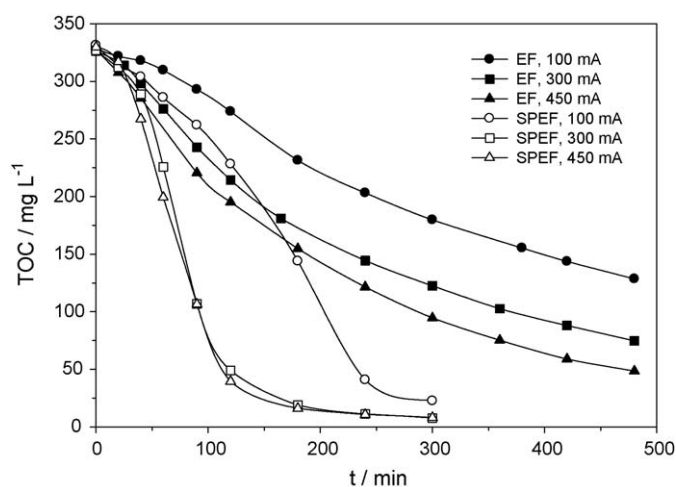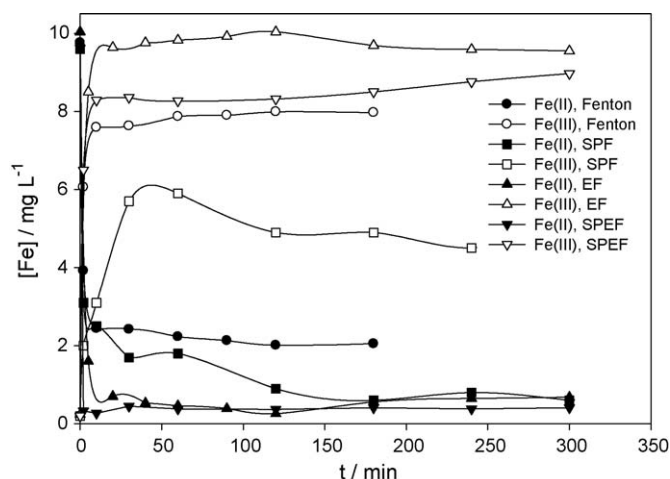

Fig. 2. TOC removal during electro-Fenton (EF) and solar photoelectro-Fenton (SPEF) treatments of 500 mg L^{-1} α-MPG, 10 mg L^{-1} Fe^{2+} and 0.05 M Na_2SO_4 solutions at pH 2.9 and 25 °C. Applied currents are indicated in the figure legend.

Fig. 4. Time course of Fe concentration. Solid symbols refer to Fe(II) and open symbols to Fe(III). Experimental conditions: ($\bigcirc$, $\bullet$) Fenton, ($\square$, $\blacksquare$) SPF, ($\triangle$, $\blacktriangle$) EF, and ($\triangledown$, $\blacktriangledown$) SPEF, with 10 mg L^{-1} Fe^{2+} (initial Fe concentration) and 500 mg L^{-1} of α-MPG. Other conditions: 300 mA and 0.05 M Na$_2$SO$_4$ (in electrochemical experiments), 72.5 mM H$_2$O$_2$ (chemical experiments), pH 2.9 and 25 °C.

obtained in chemical experiments are clearly different from those obtained in the electrochemical ones. The Fe^{2+} concentration remaining is solution is lower (clearly below 1 mg L^{-1}) in the latter case, while Fe^{3+} approaches to the initial 10 mg L^{-1} of total Fe. The data seems to suggest that the electrochemical oxidation of Fe^{2+} is more effective than the corresponding reduction of Fe^{3+}, leaving less Fe^{2+} available for direct Fenton reaction.

On the other hand, a similar positive effect of sunlight is observed for chemical and electrochemical treatments: in dark Fenton and EF experiments large mineralizations (e.g., 90% or above) are not achieved, while both SPF and SPEF systems are able to render such large organic removals.

Although increasing currents in EF and SPEF give larger TOC removals, the opposite tendency applies when considering mineralization current efficiencies (MCE), calculated by Eq. (8) [25]:

$$\text{MCE}(\%) = \frac{nFV_s\Delta(\text{TOC})_{\text{exp}}}{4.32 \times 10^7 m I t} \tag{8}$$

where n is the number of electrons consumed in the mineralization reaction of α-MPG, F is the Faraday constant (=96,487 C mol^{-1}), V_s is the solution volume (L), $\Delta(\text{TOC})_{\text{exp}}$ is the experimental TOC decay (mg L^{-1}), 4.32×10^7 is a numerical factor for unit homogenization (=3600 s h^{-1} × 12,000 mg of C mol^{-1}), m is the number of carbon atoms in an amino acid molecule (=9), I is the applied current (A) and t is the electrolysis time (h). The n-value was taken equal to 48 considering that the overall mineralization reaction of α-MPG leading to carbon dioxide and nitrate ion can be expressed according to Eq. (9):

$$C_9H_{11}NO_2 + 19H_2O \rightarrow 9CO_2 + NO_3^- + 49H^+ + 48e^- \tag{9}$$
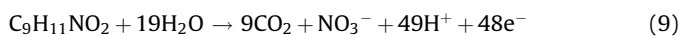
For the two configurations, the general trend is that current efficiency decreases as electrolysis is prolonged and for current rises. As an example, the MCE value after 5 h of 100 mA of EF is 90.2%, while after 5 h of the same process at 450 mA this decreases to 28.1%. Thus, large currents and prolonged electrolysis periods imply a worse use of the electrical energy. On the other hand, the presence of sunlight increases the current efficiency. Obviously, solar energy is used by the system to generate more hydroxyl radicals and to produce more reaction events, complementing the role of electrical energy. In fact, preliminary chemical experiments

by applying direct solar radiation to 500 mg L^{-1} α-MPG solutions in the presence of 10 mg L^{-1} Fe^{3+} and without H$_2$O$_2$ for 2 h showed more than 100 mg L^{-1} α-MPG removal, indicating that its Fe(III) complex undergoes direct photolysis. In some cases, current efficiencies above 100% were noticed, and the best results were always found for moderate electrolysis times of the SPEF process with low currents, e.g., an MCE-value of 216.2% was obtained after 4 h of this treatment at 100 mA.

3.2. Decay kinetics for α-MPG

Differences exist when comparing the TOC removals obtained for the four methods with the removal of the original α-MPG. Fig. 5 shows the time course of the amino acid and, as can be seen, the chemical processes give a faster α-MPG removal than their electrochemical homologues. This can be explained by taking into account that total α-MPG disappearance in the chemical processes takes place in few minutes (about 30 min for Fenton and less than 20 min for SPF), when the majority of the H$_2$O$_2$ initially added still remains in solution. The chemical systems are then particularly fast at the beginning of the reaction when large amounts of H$_2$O$_2$ are present in the solution leading to maximum HO$^\bullet$ production via Fenton reaction (1), while the electrochemical systems have lower initial reaction rates because the main oxidant H$_2$O$_2$ has to be gradually formed along time. For long reaction times, however, this trend is inverted, because the chemical processes slow-down due to the decrease in oxidant content while the electrochemical ones are enhanced by the progressive accumulation of H$_2$O$_2$ in solution. In any case, Fig. 5 makes clear that the presence of sunlight always accelerates the removal process. Blank experiments showed that the photolysis of Fe(II)-α-MPG or Fe(III)-α-MPG complexes were too slow to be compared with the removal rates derived from Fig. 5. Thus, the beneficial role of sunlight in SFP and SPEF treatments is only attributable to the existence of the PF reaction (2) enhancing HO$^\bullet$ generation in the bulk, with small participation of BDD(HO$^\bullet$) formed from reaction (5) as oxidant in the latter case.

3.3. Identification of aromatic intermediates

Aromatic intermediates formed during α-MPG degradation were identified from short-time EF trials using GC–MS and LC–MS. This method was chosen because it gives the slowest decay of the amino acid (see Fig. 5) and a larger accumulation of aromatic
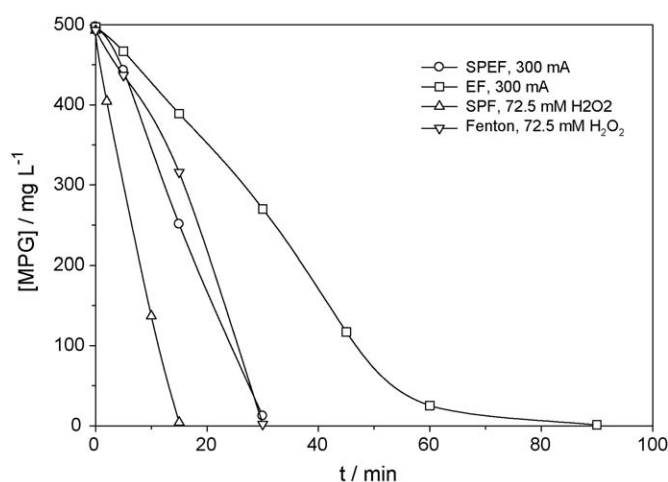
Fig. 5. α-MPG time course for the four tested oxidation processes of 500 mg L^{-1} α-MPG and 10 mg L^{-1} Fe^{2+} solutions of pH 2.9 at 25 °C. The initial H$_2$O$_2$ concentrations used for the chemical systems and the currents applied in the electrochemical ones are indicated in the legend.

Table 1
Aromatic intermediates detected during EF α-MPG degradation at 300 mA.

Aromatic compound	Analytical technique	Retention time (min)	Molecular mass (g mol^{-1})
α-MPG	GC–MS with silylation	6.9	Dimethylsilylated (O,N) 309[a]
α-Amino-hydroxy-α-methylbenzeneacetic acid[b]	LC–MS	8.6	182
α-Amino-α-methylbenzenemethanol	GC–MS with silylation	14.3	Monomethylsilylated (O) 209[a]
α-Amino-hydroxy-α-methylbenzenemethanol[b]	GC–MS with silylation	11.0	Trimethylsilylated (O,O,N) 369[a]
Acetophenone	GC–MS with silylation	9.3	Not methylsilylated 120120
	GC–MS	19.7	
o-Acetophenol	GC–MS with silylation	13.8	Monomethylsilylated (O) 208[a]
	GC–MS	23.0	136
m-Acetophenol	GC–MS	42.1	136
p-Acetophenol	GC–MS with silylation	15.0	Monomethylsilylated (O) 208[a]
	GC–MS	44.0	136
Benzoic acid	GC–MS with silylation	12.0	Monomethylsilylated (O) 194[a]
Hydroxybenzoic acid[b]	GC–MS with silylation	17.2	Dimethylsilylated (O,O) 282[a]
1-(Dihydroxyphenyl)ethanone[b]	GC–MS	44.8	152
Dihydroxybenzoic acid[b]	GC–MS with silylation	19.0	Trimethylsilylated (O,O,O) 370[a]
Phenol	GC–MS with silylation	9.0	Monomethylsilylated (O) 166[a]94
	GC–MS	27.5	
o-Hydroxyphenol	GC–MS with silylation	13.0	Dimethylsilylated (O,O) 254[a]
m-Hydroxyphenol	GC–MS with silylation	13.9	Dimethylsilylated (O,O) 254[b]
p-Hydroxyphenol	GC–MS with silylation	14.1	Dimethylsilylated (O,O) 254[a]

[a] Value corresponding to the corresponding methylsilylated derivative. Its silylation positions are indicated in the parenthesis.
[b] Compound proposed from its molecular mass and fragmentation.

intermediates that disappear at nearly the same time than the starting compound. Table 1 summarizes all the compounds detected with each analytical technique, along with their retention time and molecular mass. Note that some hydroxylated products were proposed from their molecular mass and fragmentation, without being possible to ascertain the exact position of –OH groups, whereas the data of well-defined compounds agreed with those supplied by the NIFT05 online library.

From data of Table 1, a plausible degradation pathway for α-MPG under EF conditions is proposed in Fig. 6, where the main oxidant is HO$^{\bullet}$ formed from Fenton's reaction (1) and in smaller extent BDD(HO$^{\bullet}$) produced from reaction (5). The initial attack of α-MPG with these radicals leads to three paths involving direct hydroxylation of aromatic ring, decarboxylation of the 2-amino-propionic group or its direct deammination. The former path yields α-amino-hydroxy-α-methylbenzeneacetic acid, which is decarboxylated to the corresponding α-amino-hydroxy-α-methylben-zenemethanol. This species is further deamminated to o-, m- and p-acetophenol, followed by hydroxylation to generate 1-(dihydrox-yphenyl)ethanone. The hydrogen abstraction and oxidation from
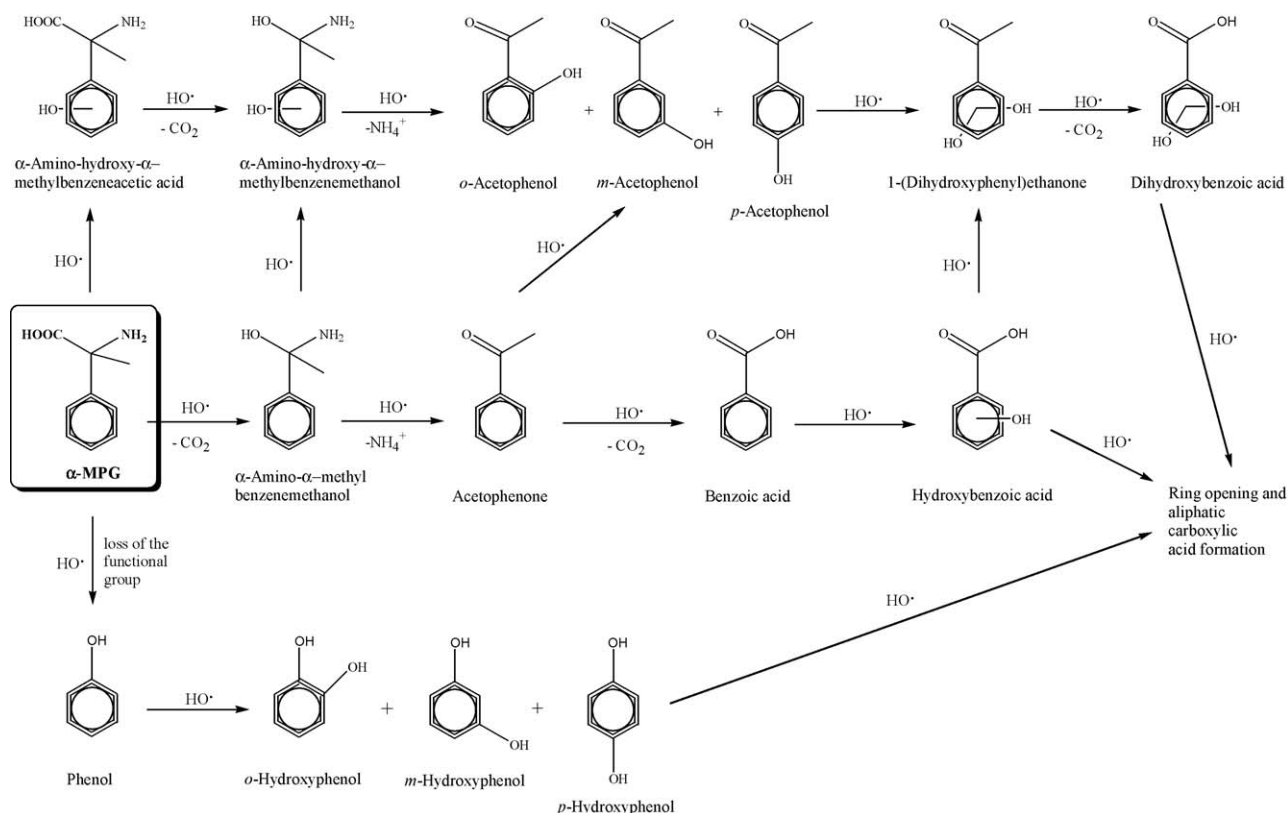
Fig. 6. Proposed reaction pathways for α-MPG degradation to aromatic by-products under EF conditions.

HO• with subsequent decarboxylation of the latter to dihydroxybenzoic acid is postulated [34]. The second path originates 1-amino-1-phenylethanol, which can be subsequently hydroxylated to (1-amino-1-hydroxyethyl)phenol or transformed into acetophenone. The latter compound can also undergo hydroxylation leading to the acetophenol isomers or decarboxylation to benzoic acid [34] that is then hydroxylated to hydroxybenzoic acid and further, to dihydroxybenzoic acid. In the third path, the functional group loss takes place, giving phenol, which is converted into its three possible hydroxylated derivatives. Degradation paths proposed in Fig. 6 could be extended to Fenton, SPF and SPEF treatments, since the same aromatic intermediates are expected to be formed in such chemical and electrochemical processes because HO• is always the main oxidant in both configurations.

3.4. Detection and evolution of carboxylic acids

As suggested in the reaction pathway of Fig. 6, the aromatic ring finally opens up to mainly generate carboxylic acids. The presence of these by-products is of relevance due to their tendency to form Fe(III) complexes that are able to absorb photons and to produce photolysis events that give an extra organic degradation pathway. The presence of these acids was corroborated by carrying out ion-exclusion HPLC analysis of all degraded solutions. Table 2 shows the different carboxylic acids identified along the four studied oxidation processes. Some of their methylsilyl derivatives were also detected during the GC–MS analysis of solutions treated during 40 min by EF. Low concentrations of the majority of those acids were always found, the exception being oxalic and oxamic acids with maximum concentrations around 20 and 40 mg L^{-1}, respectively. The former can be produced from the cleavage of longer carboxylic acids [17,21,22,24,25], while the latter could proceed from the oxidation of the 2-aminopropionic group lost during phenol formation.

Fig. 7a and b shows the time course of those acids during SPF and SPEF experiments. As can be seen, in all cases the general trend corresponds to that expected for a reaction intermediate evolution profile: an initial accumulation of the acid, a concentration maximum at intermediate times, and a decrease and final disappearance. It has to be remarked that in dark experiments (Fenton and EF, data not shown) both acids keep increasing concentrations during the treatment time and final disappearance was not observed. In fact, it is known [24,35] that both carboxylic acids are slowly removed under the experimental conditions of several AOPs, in agreement with the accumulation observed in dark Fenton and EF reactions. In this sense, the photoactivity of the Fe(III)–oxalate and Fe(III)–oxamate complexes seems to be essential for a fast removal of the two acids.

Data of Fig. 7a concerning oxalic acid evolution during SPF treatment show that a larger initial H$_2$O$_2$ content involves lower acid concentrations and a concentration maximum that appears earlier on time. Obviously, the presence of more oxidant implies a faster oxidation of all intermediates that are previous to oxalic appearance, but it also implies a faster oxidation of oxalic acid itself. Nevertheless, this behaviour is different during the SPEF treatment, where lower concentration and slower destruction are noticed at 100 mA, whereas at 300 mA a maximum acid concentration with a strong decrease in its disappearance time is found, being even shorter at 450 mA. This difference could be explained by the different oxidant supply pattern used in both techniques: in SPF all H$_2$O$_2$ is initially added to solution while in SPEF H$_2$O$_2$ is steadily produced. In addition, increasing BDD(HO•) production with increasing current in SPEF also favours the destruction of oxalic acid. Oxamic acid time profiles depicted in Fig. 7b are similar to those of oxalic acid in Fig. 7a, although with concentration maxima appearing later, as expected if Fe(III)–
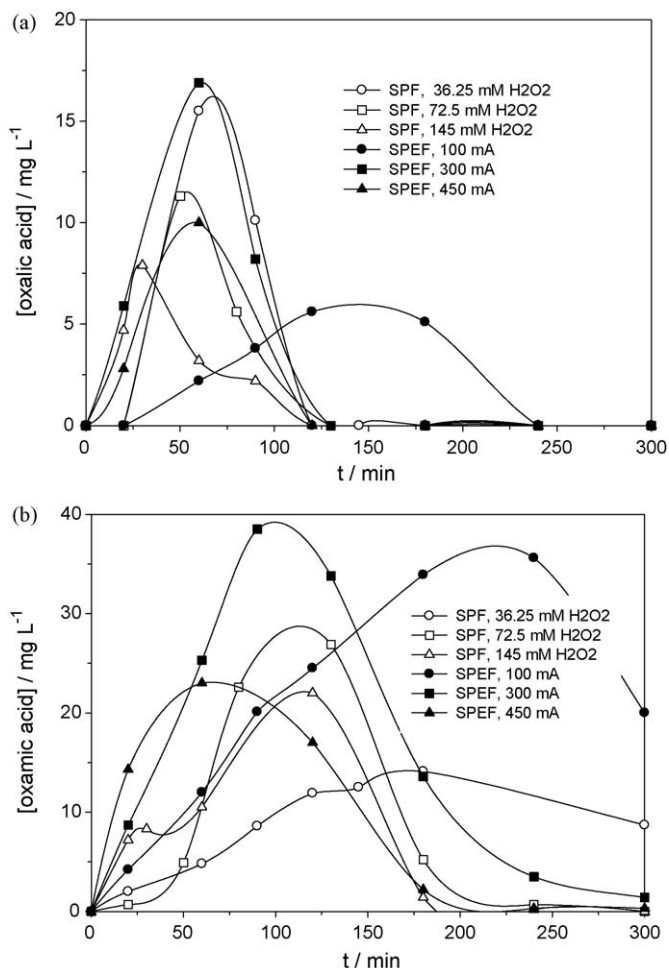

Fig. 7. (a) Oxalic and (b) oxamic acid concentration along time in SPF and SPEF experiments of 500 mg L^{-1} α-MPG and 10 mg L^{-1} Fe^{2+} solutions at pH 2.9 and 25 °C. The initial H$_2$O$_2$ concentrations used for the chemical system and the currents applied in the electrochemical one are indicated in the legend.
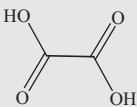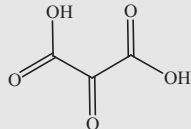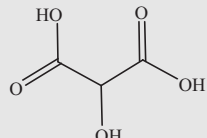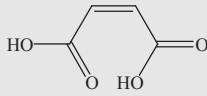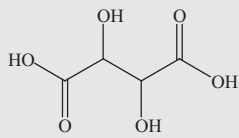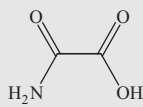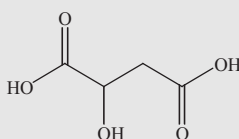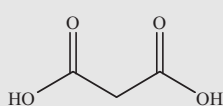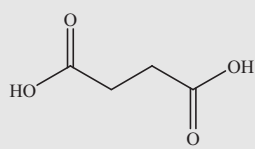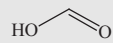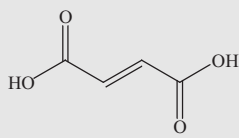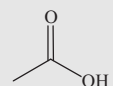
oxamate complexes are more slowly formed and more hardly oxidized and photolyzed. This indicates the existence of alternative oxidation pathways with –NH$_2$ group release from the α-MPG molecule taking place at different times.

A simple mass balance of carbon shows that even when oxalic and oxamic acids have been completely removed some residual organics remain in solution. This can be deduced, for example, after 5 h of the SPEF treatment at 300 mA (see Fig. 2) since 97.5% mineralization is attained with a residual TOC of 7.7 mg L^{-1}. This means that small amounts of other undetected by-products, more recalcitrant than carboxylic acids, are formed during α-MPG degradation.

3.5. Nitrogen mass balance

The fate of the nitrogen originally present in the α-MPG molecule should be an inorganic form containing the heteroatom. Indeed, the detection of N-containing organic reaction intermediates, like oxamic acid, is possible, but in the absence of noticeable TOC dissolved inorganic species like NH$_4^+$, NO$_2^-$ and NO$_3^-$ should account for the main part of nitrogen. Thus, quantification of those ions was carried out for the four oxidation processes. Fig. 8a depicts the time course of NH$_4^+$ during SPF and SPEF experiments, while Fig. 8b contains the data corresponding to the NO$_3^-$ ion. NO$_2^-$ ion was not detected, something predictable for a rather unstable ion in strong oxidant media. Comparing both figures, it is clear that the

Table 2
Carboxylic acids detected during Fenton and EF α-MPG oxidation, in dark and sunlight irradiated experiments.

Carboxylic acid	Molecular formula	Analytical technique	Retention time (min)	Molecular mass (g mol^{-1})
Oxalic acid		HPLC	6.1	90
Mesoxalic acid		HPLC	6.3	118
Tartronic acid		HPLC GC–MS with silylation	7.3 10.2	120 336[a]
Maleic acid		HPLC GC–MS with silylation	7.5 9.9	116 260[b]
Tartaric acid		HPLC GC–MS with silylation	8.0 16.7	140 438[c]
Oxamic acid		HPLC	8.5	89
Malic acid		HPLC GC–MS with silylation	9.0 10.5	134 350[a]
Malonic acid		HPLC GC–MS with silylation	10.5 8.0	104 248[b]
Succinic acid		HPLC GC–MS with silylation	11.2 10.1	118 262[b]
Formic acid		HPLC	13.0	
Fumaric acid		HPLC GC–MS with silylation	14.0 10.8	116 260[b]
Acetic acid		HPLC	14.3	46

[a] Value corresponding to the trimethylsilyl derivative detected after 40 min of EF treatment at 300 mA.
[b] Value corresponding to the dimethylsilyl derivative detected after 40 min of EF treatment at 300 mA.
[c] Value corresponding to the tetramethylsilyl derivative detected after 40 min of EF treatment at 300 mA.
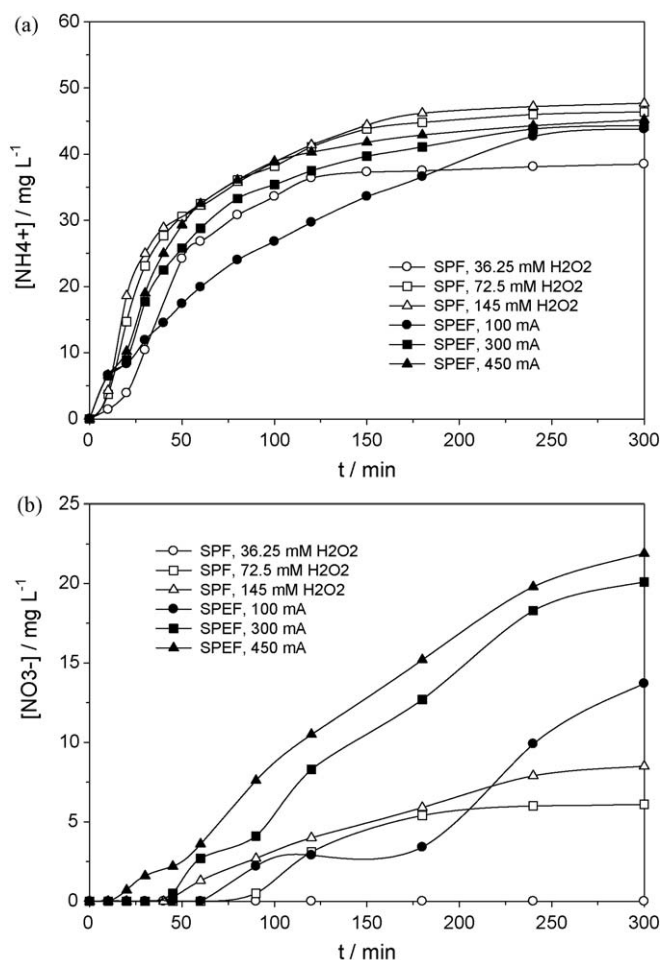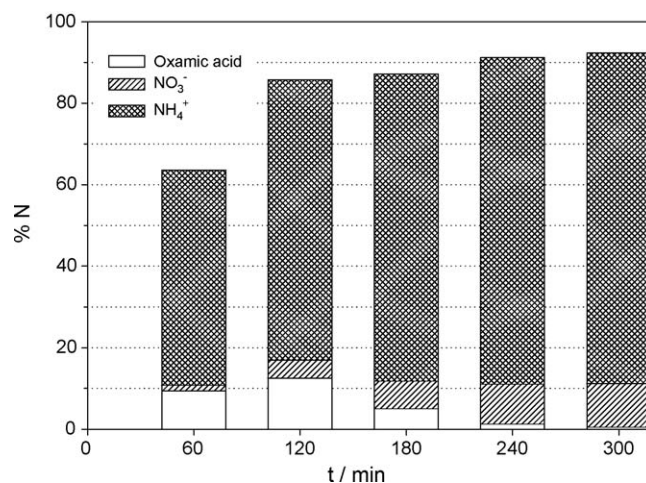
Fig. 8. (a) NH_4^+ and (b) NO_3^- concentrations along time detected under the same experimental conditions of Fig. 5.

Fig. 9. Percentages of nitrogen corresponding to the detected oxamic acid, NH_4^+, and NO_3^- at different reaction times of the solar photoelectro-Fenton treatment of a 500 mg L^{-1} α-MPG solution with 10 mg L^{-1} Fe^{2+} at pH 2.9, 300 mA and 25 °C.

amount of NH_4^+ present in solution is always larger than the amount of NO_3^-, in agreement with the resistance to oxidation of the former [36]. It is also worth to notice that the main part of NH_4^+ appears in solution during the first 2 h of reaction, while the NO_3^- accumulation in solution takes place at longer time, as expected for a sequential oxidation of NH_4^+ to NO_3^-. The rather fast accumulation of NH_4^+ in solution agrees with the existence of early deammination steps, as proposed in the degradation paths of Fig. 6. As can be seen in Fig. 8a and b, stronger oxidation conditions (more initial H_2O_2 in SPF or larger currents in SPEF) involve larger NH_4^+ and NO_3^- productions. Something similar can be said when comparing data concerning dark (not shown) and irradiated experiments, being the presence of sunlight beneficial for the faster production of those ions because more mineralization degree is attained.

An attempt to close the N mass balance was carried out by taking into account the three main N-species, i.e., oxamic acid, NH_4^+ and NO_3^-. Fig. 9 is a bar chart where the percentages of each of those species detected along the SPEF degradation at 300 mA are displayed. As can be seen, the main nitrogen species present in the solution is NH_4^+, oxamic acid is only a minor intermediate in the oxidation pathway, and NO_3^-, the expected final product, is only obtained in relatively small quantities. It is also remarkable that mass balance is never closed. Even after 300 min reaction, when only 7.7 mg L^{-1} of TOC remain in solution, the sum of the nitrogen contained in the three species is 92.3% of the total expected. The rest of nitrogen (7.7%) could be lost as volatile nitrogen species like NO_x [37].

4. Conclusions

The oxidation of α-MPG in aqueous solution has been carried out by means of Fenton, solar photo-Fenton, electro-Fenton, and solar photoelectro-Fenton processes in the presence of several initial H_2O_2 concentrations or different currents. Faster reaction rates are obtained for the electrochemical processes, especially for TOC removal, although little can be said about the efficiency of each process with respect to H_2O_2 consumption because the assessment of the amount of oxidant generated during the electrochemical experiments is not easy. The presence of sunlight always improves the oxidation efficiencies, mainly due to the role played by the photo-Fenton reaction and the existence of direct photolysis of the Fe(III) complexes formed with reaction intermediates. Aromatic intermediates were detected using GC–MS and LC–MS analysis and a comprehensive degradation pathway to aromatic intermediates that involves the hydroxyl radical as the main oxidant species is proposed. HPLC and GC–MS analysis was performed for the detection and quantification of generated carboxylic acids, being oxalic and oxamic acids those detected at higher concentrations. Ion chromatography was used to quantify inorganic species such as NH_4^+ and NO_3^-, the nitrogen containing inorganic species detected. The nitrogen mass balance was not closed, probably due to the generation of NO_x or other volatile nitrogen species.

References

[1] R. Andreozzi, V. Caprio, A. Insola, R. Marotta, Catal. Today 53 (1999) 51–59.
[2] S. Parsons (Ed.), Advanced Oxidation Processes for Water and Wastewater Treatment, IWA Publishing, London, 2004.
[3] M. Pera-Titus, V. García-Molina, M.A. Baños, J. Giménez, S. Esplugas, Appl. Catal. B: Environ. 47 (2004) 219–256.
[4] J.J. Pignatello, E. Oliveros, A. MacKay, Crit. Rev. Environ. Sci. Technol. 36 (2006) 1–84.
[5] S.H. Bossmann, E. Oliveros, M. Kantor, S. Niebler, A. Bonfill, N. Shahin, M. Wörner, A.M. Braun, Water Sci. Technol. 49 (2004) 75–80.
[6] J.J. Pignatello, Environ. Sci. Technol. 26 (1992) 944–951.

[7] R.G. Zepp, B.C. Faust, J. Hoigné, Environ. Sci. Technol. 26 (1992) 313–319.
[8] G. Ruppert, R. Bauer, G. Heisler, J. Photochem. Photobiol. A: Chem. 73 (1993) 75–78.
[9] R. Bauer, H. Fallmann, Res. Chem. Intermed. 23 (1997) 341–354.
[10] Y. Zuo, J. Hoigné, Environ. Sci. Technol. 26 (1992) 1014–1022.
[11] M.A. Oturan, J.J. Aaron, N. Oturan, J. Pinson, Pestic. Sci. 55 (1999) 558–562.
[12] M.A. Oturan, J. Appl. Electrochem. 30 (2000) 477–478.
[13] B. Boye, M.M. Dieng, E. Brillas, Environ. Sci. Technol. 36 (2002) 3030–3035.
[14] E. Brillas, B. Boye, M.M. Dieng, J. Electrochem. Soc. 150 (2003) E583–E589.
[15] E. Guivarch, S. Trévin, C. Lahitte, M.A. Oturan, Environ. Chem. Lett. 1 (2003) 38–44.
[16] N. Oturan, M.A. Oturan, Agron. Sustain. Dev. 25 (2005) 267–270.
[17] S. Irmak, H.I. Yavuz, O. Erbatur, Appl. Catal. B: Environ. 63 (2006) 243–248.
[18] C. Flox, S. Ammar, C. Arias, E. Brillas, A.V. Vargas-Zavala, R. Abdelhedi, Appl. Catal. B: Environ. 67 (2006) 93–104.
[19] M. Diagne, N. Oturan, M.A. Oturan, Chemosphere 66 (2007) 841–848.
[20] I. Sirés, J.A. Garrido, R.M. Rodríguez, E. Brillas, N. Oturan, M.A. Oturan, Appl. Catal. B: Environ. 72 (2007) 382–394.
[21] I. Sirés, N. Oturan, M.A. Oturan, R.M. Rodríguez, J.A. Garrido, E. Brillas, Electrochim. Acta 52 (17) (2007) 5493–5503.
[22] I. Sirés, F. Centellas, J.A. Garrido, R.M. Rodríguez, C. Arias, P.L. Cabot, E. Brillas, Appl. Catal. B: Environ. 72 (2007) 373–381.
[23] M. Panizza, G. Cerisola, Electrochim. Acta 51 (2005) 191–199.
[24] C. Flox, J.A. Garrido, R.M. Rodríguez, P.L. Cabot, F. Centellas, C. Arias, E. Brillas, Catal. Today 129 (2007) 29–36.
[25] C. Flox, P.L. Cabot, F. Centellas, J.A. Garrido, R.M. Rodríguez, C. Arias, E. Brillas, Appl. Catal. B: Environ. 75 (2007) 17–28.
[26] Real Decreto 849/1986. Reglamento del Dominio Público Hidráulico. Spanish B.O.E. n°. 103 of 30th April, Madrid. (1986).
[27] I. Oller, S. Malato, J.A. Sánchez-Pérez, M.I. Maldonado, W. Gernjak, L. Pérez-Estrada, Water Sci. Technol. 55 (2007) 229–235.
[28] S. Malato, J. Blanco, M.I. Maldonado, I. Oller, W. Gernjak, L. Pérez-Estrada, J. Hazard. Mater. 146 (2007) 440–447.
[29] I. Oller, S. Malato, J.A. Sánchez-Pérez, W. Gernjak, M.I. Maldonado, L. Pérez-Estrada, C. Pulgarín, Catal. Today 122 (2007) 150–159.
[30] I. Oller, P. Fernández-Ibáñez, M.I. Maldonado, L. Pérez-Estrada, W. Gernjak, C. Pulgarín, P.C. Passarinho, S. Malato, Res. Chem. Intermed. 33 (2007) 407–420.
[31] F.J. Welcher (Ed.), Standard Methods of Chemical Analysis, vol.2, part B, 6th ed., R.E. Krieger Pub. Co., New York, 1975, p. 1827.
[32] J.G. Calvert, J.N. Pitts, Photochemistry, Wiley, New York, 1967, pp. 783–786.
[33] X. Domènech, J.A. Ayllón, J. Peral, J. Rieradevall, Environ. Sci. Technol. 36 (2006) 5517–5520.
[34] C. Walling, Acc. Chem. Res. 8 (1975) 125–131.
[35] R. Alnaizy, A. Akgerman, Adv. Environ. Res. 4 (2000) 233–244.
[36] A. Bravo, J. García, X. Domènech, J. Peral, J. Chem. Res. (1993) 376–377.
[37] D. Vione, C. Minero, V. Maurino, E. Pelizzetti, Environ. Sci. Pollut. Res. 14 (2007) 241–243.